Closure of the stop-band in photonic wire Bragg gratings

M. Gnan[1], W. C. L. Hopman[2], G. Bellanca[3], R. M. de Ridder[4], R. M. De La Rue[5], and P. Bassi[1]

[1]*Dipartimento di Elettronica, Informatica e Sistemistica, University of Bologna, Viale Risorgimento 2, I 40136 Bologna, Italy*
[2]*Sensata Technologies, Kolthofsingel 8, 7602 EM Almelo, The Netherlands*
[3]*Dipartimento di Ingegneria, University of Ferrara, Via Saragat 1, I 44100 Ferrara, Italy*
[4]*University of Twente, MESA$^+$ Institute, IOMS group, P.O. Box 217, 7500 AE Enschede, The Netherlands*
[5]*Department of Electronics and Electrical Engineering, University of Glasgow, G12 8LT Glasgow, United Kingdom*

marco.gnan@unibo.it

Abstract: Photonic Wire Bragg Gratings, made by periodic insertion of lateral rectangular recesses into photonic wires in silicon-on-insulator, can provide large reflectivity with short device lengths because of their large index contrast. This type of design shows a counter-intuitive behaviour, as we demonstrate — using experimental and numerical data — that it can have low or null reflectance, even for large indentation values. We provide physical insight into this phenomenon by developing a model based on Bloch mode theory, and are able to find an analytical expression for the frequency at which the grating does not sustain the stop-band. Finally we demonstrate that the stop-band closing effect is a general phenomenon that may occur in various types of periodic device that can be modeled as transmission line structures.

OCIS codes: (230.1480) Bragg Reflector; (130.5296) Photonic Crystal Waveguides

References and links

1. M. Lipson, "Guiding, modulating, and emitting light on Silicon — Challenges and opportunities," J. Lightwave Technol. **23**, 4222–4238 (2005).
2. B. Jalali and S. Fathpour, "Silicon photonics," J. Lightwave Technol. **24**, 4600–4615 (2006).
3. S. Noda, "Recent progresses and future prospects of two- and three-dimensional photonic crystals," J. Lightwave Technol. **24**, 4554–4567 (2006).
4. P. Velha, E. Picard, T. Charvolin, E. Hadji, J. C. Rodier, P. Lalanne, and D. Peyrade, "Ultra-high Q/V Fabry-Perot microcavity on SOI substrate," Opt. Express **15**, 16090–16096 (2007).
5. A. R. Md Zain, N. P. Johnson, M. Sorel, and R. M. De La Rue, "Ultra high quality factor one dimensional photonic crystal/photonic wire micro-cavities in silicon-on-insulator (SOI)," Opt. Express **16**, 12084–12089 (2008).
6. M. Gnan, G. Bellanca, H. Chong, P. Bassi, and R. M. De La Rue, "Modelling of photonic wire Bragg gratings," Opt. Quantum Electron. **38**, 133–148 (2006).
7. A. S. Jugessur, J. Dou, S. Aitchison, R. M. De La Rue, and M. Gnan, "A photonic nano-Bragg grating device integrated with microfluidic channels for bio-sensing applications," Microelectron. Eng. (in press, 2009).
8. P. Yeh and A. Yariv, *Optical Waves in Crystals* (Wiley, 1984).
9. D. M. Atkin, P. S. J. Russell, T. A. Birks, and P. J. Roberts, "Photonic band structure of guided Bloch modes in high index films fully etched through with periodic microstructure," J. Mod. Opt. **43**, 1035–1053 (1996).
10. F. Riboli, P. Bettotti, and L. Pavesi, "Band gap characterization and slow light effects in one dimensional photonic crystals based on silicon slot-waveguides," Opt. Express **15**, 11769–11775 (2007).

#107611 - $15.00 USD Received 17 Feb 2009; revised 2 May 2009; accepted 4 May 2009; published 12 May 2009

11. M. Gnan, S. Thoms, D. S. Macintyre, R. M. De La Rue, and M. Sorel, "Fabrication of low-loss photonic wires in silicon-on-insulator using Hydrogen Silsesquioxane electron-beam resist," Electron. Lett. **44**, 115–116 (2008).
12. F. Fogli, N. Greco, P. Bassi, G. Bellanca, P. Aschieri, and P. Baldi, "Spatial harmonics modelling of planar periodic segmented waveguides," Opt. Quantum Electron. **33**, 485–498 (2001).
13. P. Bienstman and R. Baets, "Optical modelling of photonic crystals and VCSELs using eigenmode expansion and perfectly matched layers," Opt. Quantum Electron. **33**, 327–341 (2001).

1. Introduction

Silicon-on-insulator (SOI) is the key platform with the potential for merging photonics with silicon microelectronics, because of its compatibility with CMOS processes — and because of the small footprint given by the high refractive-index contrast, which gives the potential for low-cost, mass-market, high-bandwidth and compact devices [1, 2]. On the SOI platform, photonic crystal [3] and photonic wire structures can provide the basis for integrated optical circuits. Photonic wires, as well as having the basic function of routing light throughout the chip, can also provide wavelength selective functionalities (e.g. Bragg gratings) by engineering a periodic variation of the refractive index into their core or cladding. Thanks to the high refractive-index contrast of SOI, high reflectivity gratings as short as a few tens of micrometres can be fabricated for example by carving circular holes along the wire [4, 5] or by the insertion of periodic indentation on the sidewalls [6, 7]. Although not studied as extensively, the latter grating design (the photonic wire Bragg grating — PhWBG) has the advantage of facilitating a better flow and interaction with fluids, due to the exposed teeth (rather than laterally enclosed holes) resulting in easier fabrication (reduced RIE-lag effect), and better sensing performance [7]. A typical structure of this kind, obtained through the periodic insertion of rectangular recesses on both sides of the photonic wire, is shown in Fig. 1.

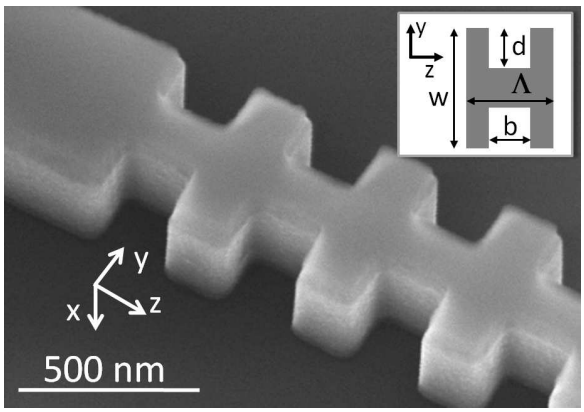

Fig. 1. Scanning electron micrograph giving a 'bird's-eye' view of photonic wire Bragg grating fully etched into silicon waveguide core layer. Inset: top view, defining dimensions.

In a previous publication [6], using a 3D finite-difference time-domain (FDTD) approach, we have studied numerically the properties of the stop-band of PhWBG in the wavelength region around 1.55 μm and found that, over a range of geometrical dimensions corresponding to large refractive index modulation, the gratings show an unexpected reduction in the stop-bandwidth and reflectance intensity. This phenomenon is counter-intuitive, since the reflectivity is usually expected to increase with increasing magnitude in the refractive index modulation as shown, for example, in [8] — when using Bloch and coupled-mode theories.

Little scientific literature appears to exist on this subject. The majority of publications deals with gratings made by inserting periodic circular hole patterns into the photonic wires (see [4, 5]

#107611 - $15.00 USD Received 17 Feb 2009; revised 2 May 2009; accepted 4 May 2009; published 12 May 2009

and references therein) — but in this case such a phenomenon appears not to have been reported. The effect is however cursorily mentioned in two papers [9,10] that report theoretical results obtained on structures with a geometry having some similarity to ours, being also based on straight edges and square corners. In [9], Atkin *et al.* analyse a 2D grating geometry made by full on-off variation of the refractive index. They perform a theoretical and numerical study that assesses the features of this new type of structures. In their analysis they encounter a phenomenon of disappearance of the stop-band in a periodic structure, which they relate to Brewster angle incidence. In [10], Riboli *et al.* develop a 3D numerical investigation of gratings based on a slot waveguide geometry. They report on many structures that exhibit this phenomenon, but do not deepen their analysis.

From an experimental point of view, this intriguing phenomenon seems worthy of further attention because of the possibility of producing stimulus-controlled closure or opening of the band-gap. Also, we envision that for bio-sensing applications, fluid flowing in the grating tooth gap could be sensed by detection of the tuning the stop-band closure condition. Regarding microcavities based on such gratings, the closure of the stop-band effect could be useful in the design of tapering sections between grating and wire waveguides that could provide modal shape tapering without introducing further Bragg reflection conditions.

In this paper we report experimental results that confirm the closure of the stop-band for this structure — and show close agreement with 3D time-domain numerical simulations (section 2). In section 3 we provide a theoretical explanation that starts with a 1D model and extends to a 3D one, finding an analytical expression that predicts the closure frequency of the stop-band. Finally, in section 4, we highlight the essential features of the phenomenon by designing a structure that deliberately includes the stop-band closure effect within a transmission-line model.

2. Experimental evidence of band-gap closure

The geometry of the Photonic Wire Bragg Gratings (PhWBG), as sketched in Fig. 1, is obtained through the periodic insertion of rectangular recesses on both sides of a photonic wire made out of silicon ($n_{Si} = 3.479$) on thermal silicon oxide ($n_{SiO_2} = 1.445$). We used SOI material patterned with hydrogen silsesquioxane (HSQ) and e-beam and selectively transferred into silicon with dry-etching [11]. The thickness values of the silicon core and silica lower cladding layers were 260 nm and 1 μm, respectively. The experimental transmission of the devices was measured in the 1100–1700 nm wavelength range for only the TE polarization, thanks to a broadband source combined with an optical spectrum analyser (with a window of 5 nm) arranged in an end-fire set-up.

The nominal dimensions of the gratings were: period $\Lambda = 390$ nm and gap length $b = 195$ nm. The recess depth d was swept from 0 (no indentation) to $w/2$ (fully on-off grating). Photonic wires as wide as the grating itself ($w = 500$ nm) were employed as input and output feeder waveguides.

To investigate the occurrence of band-gap closure, we firstly studied the experimental transmission of a set of 40-period long PhWBGs. The geometry that results in a closed band-gap would have a transmittance that lacks the Bragg feature.

Figure 2 reports three of the experimental spectra of 40-period long gratings that show evidence of the disappearance of the stop-band. At $d = 160$ nm, the transmission shows a stop-band dip centred approximately at $\lambda \approx 1385$ nm. Increasing d by 10 nm results in the dip being absent and a further 10 nm increase shows the dip again, centred at $\lambda \approx 1340$ nm.

The experimental study was completed by a 3D FDTD numerical investigation of gratings having nominal geometries identical to those of the fabricated set. The simulated gratings were designed as short as 16 periods, as a trade-off between computational load and visibility of the

#107611 - $15.00 USD Received 17 Feb 2009; revised 2 May 2009; accepted 4 May 2009; published 12 May 2009

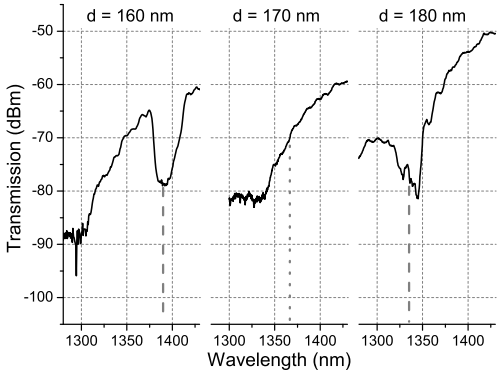

Fig. 2. Experimental transmission curves for three recess depth (d) values (other dimensions are given in the main text). For recess depth $d = 160$ nm the main stop-band is centered at ≈ 1385 nm. The higher order stop-band is also visible at wavelengths smaller than 1320 nm (compare with Fig. 3). For $d = 170$ nm the main stop-band is not visible (the dotted line points to its expected centre). For $d = 180$ nm the stop-band is again visible centered approximately at 1340 nm. Also the higher order stop-band is shifted to smaller wavelengths and does not appear in the graph. Note that the overall slope of all the curves is mainly due to the characteristic of the light source employed.

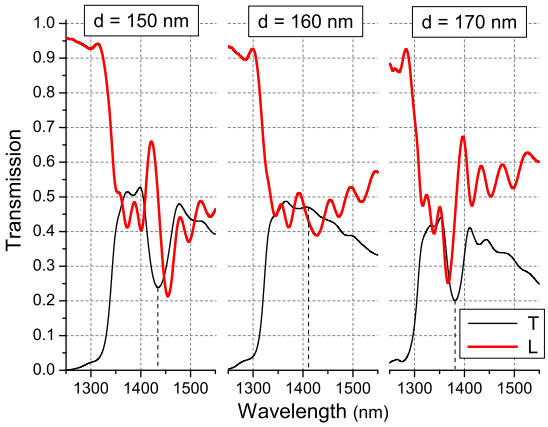

Fig. 3. Calculated Transmission (T) and Loss (L) spectra (obtained as $L = 1 - (T + R)$, R standing for Reflectance) relevant to three geometrical configurations. For recess depth $d = 160$ nm, the stop-band disappears. Note the opposite slope of the loss curve within the stop-band region for $d = 150$ nm and $d = 170$ nm. The gratings are 16-periods long.

#107611 - $15.00 USD Received 17 Feb 2009; revised 2 May 2009; accepted 4 May 2009; published 12 May 2009

main effects [6].

Figure 3 shows the calculated transmission (T) and loss (L) curves (obtained as $L = 1-(T+R)$, with R standing for reflectance) relevant to the geometrical configurations that show evidence of the disappearance of the stop-band for TE polarization. On the whole, the transmission (black) curves reproduce the experimental ones of Fig. 2 — showing shallower stop-bands because of the smaller device length. At $d = 150$ nm the grating shows a stop-band with minimum transmission at $\lambda_0 \approx 1435$ nm — and losses that decrease with the wavelength, within the stop-band. At $d = 160$ nm, the stop-band is barely discernible around $\lambda_0 \approx 1420$ nm and, at $d = 170$ nm, the stop-band opens again with a transmission minimum at $\lambda_0 \approx 1380$ nm. We note that for this geometry, within the stop-band, the slope of loss curve is opposite to that of the initial configuration.

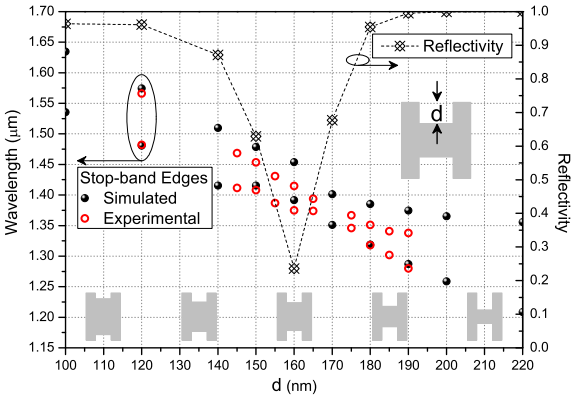

Fig. 4. Positions of numerical (black filled circles) and experimental (red empty circles) transmission stop-band of PhWBG in dependence on the recess depth d. The reduction of stop bandwidth is consistent the reduction of numerical maximum reflectance (crossed diamonds)

Finally, the results of both studies are summarised in Fig. 4, which reports the experimental (empty circles) and numerical values (filled circles) of the stop-band edges as a function of the recess depth d. The positions of the edges shift to shorter wavelength values as the average effective index of the grating decreases for increasing d. On the whole, the numerical data points define larger stop-bands, because of the lower spectral selectivity of the shorter gratings. As already demonstrated, experimentally the stop-band disappears at $d = 170$ nm, where no empty circles could be drawn — whereas numerical simulations suggest the disappearance is at $d \approx 160$ nm. The magnitude of the overall deviation between experimental and numerical data is consistent with the previously demonstrated large sensitivity to the geometrical dimensions [11].

Figure 4 also shows that the numerically evaluated reflectance values (crossed diamonds), obtained as the maximum value within the stop-band [6], behave consistently with the reduction of the gap widths, having a minimum at $d = 160$ nm.

In conclusion, experimental and numerical data confirm that the stop-band may disappear even where the geometry deformation is large: a grating having a variation of width of 64% ($d = 160$ nm) has the same reflectivity as one that has an 8% variation ($d = 20$ nm) [6]. Furthermore, the reduction of the stop-band width is accompanied by a reduction of reflectivity and an inversion of the slope of the loss curve within the stop-band. It is then worthwhile to develop a deeper theoretical analysis by providing a model that can explain not only why this happens, but also tell whether and where the stop-band will disappear.

#107611 - $15.00 USD Received 17 Feb 2009; revised 2 May 2009; accepted 4 May 2009; published 12 May 2009

3. Theoretical model

In order to develop the theoretical model we shall follow the steps depicted in Fig. 5, starting from (a) the analysis of a 1D interface between two media, (b) building a 1D-stack grating by periodically repeating the interface, (c) defining a 2D grating through the insertion of lateral confinement, and finally (d) building the PhWBG by drawing a symmetry plane within a cladding layer.

Considering the interface between two semi-infinite media (having refractive indices n_1 and n_2 respectively) depicted in Fig. 5(a), in each homogeneous region the field is expressed as plane waves and is characterised by the dispersion relation given by the wave equation. TE polarised waves have the electric field component parallel to the x axis, whereas TM polarised waves have the magnetic field component parallel to the x axis.

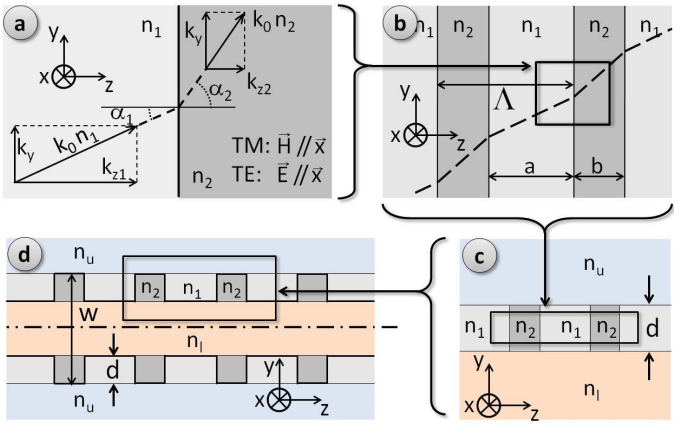

Fig. 5. Sketch of the steps of the theoretical model. (a) Semi-infinite interface. (b) 1D-stack grating. (c) Laterally confined 2D grating. (d) Photonic Wire Bragg Grating.

Refraction and reflection occur at the interface. It is well known that the refraction (transmission) coefficient always remains positive for both polarizations, whereas, for non-magnetic materials, only the TM reflection coefficient can become null and negative. Its expression is:

$$\rho = \frac{n_2 \cos(\alpha_1) - n_1 \cos(\alpha_2)}{n_1 \cos(\alpha_2) + n_2 \cos(\alpha_1)} , \tag{1}$$

which vanishes when $\alpha_1 + \alpha_2 = \pi/2$, at the Brewster's angle. If the propagation direction is reversed, the reflection coefficient changes its sign: ρ_L of the wave coming from the left with incidence angle α_1 is opposite to that of a wave coming from the right (ρ_R) with incidence angle α_2: $\rho_L = -\rho_R$.

It is convenient to re-arrange Eq. (1) so as to involve only quantities that do not depend on the considered layer, being conserved at the interface. As shown in appendix A, the Brewster condition implies proportionality between the vacuum wavenumber k_0 and the transverse wavenumber k_y according to

$$k_y = k_0 \left(\sqrt{\frac{1}{n_1^2} + \frac{1}{n_2^2}} \right)^{-1} \equiv k_0 \, n_B , \tag{2}$$

where n_B is the effective index as seen from the field along the transverse direction y at Brewster's condition. Note also that the sign of ρ is related to Eq. (2): it switches when k_y and k_0 switch from satisfying $k_y > k_0 n_B$ to satisfying $k_y < k_0 n_B$.

#107611 - $15.00 USD Received 17 Feb 2009; revised 2 May 2009; accepted 4 May 2009; published 12 May 2009

If a stacked structure having period Λ is considered [Fig. 5(b)], the field distribution will have the same periodicity as the structure. The dispersion equation becomes more complicated as it includes the constraints given by the Bloch theorem — and is reported in appendix B. We will refer to it as $f_{1D}(k_0, k_y, k_z) = 0$, where k_z is the Bloch wave-vector along the periodicity direction z.

When the multiple reflections of the interfaces build up in-phase, the grating develops a stop-band, the edges of which are defined by the solutions of the dispersion relation at the Bragg condition $k_z = K/2 = \pi/\Lambda$. The stop-band width depends on the strength of the reflections: the disappearance of the band-gap corresponds then to values of k_0 and k_y, which at the same time fulfill two conditions, the Brewster's relation (2) and the dispersion relation at $k_z = K/2$.

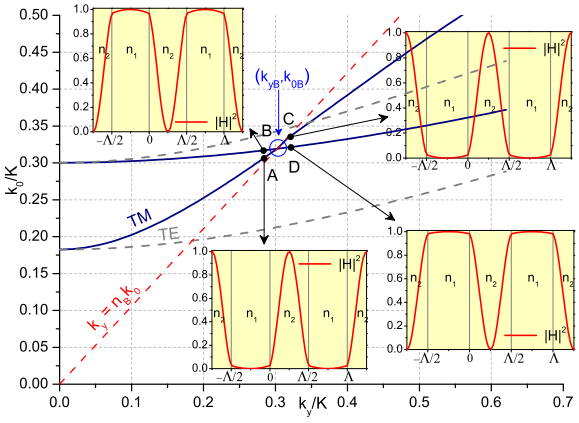

Fig. 6. Band gap edges for TM (solid blue curves) and TE (dashed gray curves) polarization together with the (dashed red) line corresponding to Brewster's condition. The insets show the normalised squared absolute value of the magnetic field $|H|^2$ for TM polarization at 4 points around the gap-closing condition. Intensity distributions A and B are calculated for $k_y = 0.2855K$, whereas C and D are calculated for $k_y = 0.3228K$.

Note that Brewster's phenomenon is independent of the geometry of the 1D grating (period, duty cycle) as shown in Eq. (2). It is anyway implicitly included in the dispersion equation of the grating, as is demonstrated by the band-gap edges for the TM (solid blue curve) and TE (dashed gray curve) polarizations shown in Fig. 6, together with the dashed red line corresponding to Brewster's condition (2). The TM edges cross each other at $(k_{yB}, k_{0B}) = (0.3024K, 0.3191K)$, a point belonging also to the Brewster line. The data in the figure are calculated for a 1D grating with $n_1 = 1$, $n_2 = 2.97$ and a 0.5 as the duty cycle.

To find the analytical expression for this crossing point, it is convenient to firstly solve $f_{1D} = 0$ at the Brewster condition and then pose the Bragg condition. As is shown in appendix B, this yields the expression of the vacuum wave-number for which the grating does not have a lowest-order stop-band:

$$k_{0B} = \frac{\pi}{\eta\, n_B}, \tag{3}$$

where $\eta = \frac{n_2}{n_1} a + \frac{n_1}{n_2} b$ — and a, b are the thicknesses of the layers of the 1D grating having refractive index n_1 and n_2, respectively. Equation (3) shows that the dispersion relation, which at the Bragg condition in general yields two distinct solutions for each stop-band order — see for example Fig. 6 at constant k_y— for simultaneous satisfaction of Brewster's angle, returns only one value k_{0B} (or k_{yB}). In other words, the dispersion curves cross and there is no stop-gap.

We shall now consider the behaviour of the standing wave patterns around the crossing point.

#107611 - $15.00 USD Received 17 Feb 2009; revised 2 May 2009; accepted 4 May 2009; published 12 May 2009

Note that, at that point, the field is not a standing wave, but rather is a travelling wave — because of the absence of any reflection. The insets of Fig. 6 show $|H_x|^2$, the squared absolute values (proportional to the intensity and normalised to 1) of the only magnetic field component for the TM polarization, which can be used to characterise the dispersion branches. The intensity distributions A and B are calculated for $k_y = 0.2855K$, whereas points C and D are calculated for $k_y = 0.3228K$.

As usual for cases of branch crossing and anti-crossing, the mode shape of the lower left branch remains similar to that of the upper right after the crossing point, and vice versa. If we compare intensity distributions A and D (both on the low-frequency band edge), representing states on opposite sides of the crossing, the locations of the maxima and minima appear to have shifted by $\Lambda/2$. The same holds for B and C, on the high-frequency band edge. The shift is due to the change of sign of the reflection coefficient when crossing the Brewster condition line. The reflected waves at all interfaces are shifted by π, thus shifting the standing wave field pattern by $\pi/2$. The intensity pattern, having half the period of the field pattern, is therefore shifted by π, which corresponds to $\Lambda/2$.

We can now increase further the complexity of the grating by creating a slab waveguide that has a periodic variation of the core refractive index, simply by adding two homogeneous semi-infinite layers (upper n_u and lower n_l), having interfaces parallel to the periodicity direction z — and separated by a distance d [Fig. 5(c)].

Similarly to the classical slab waveguide having a uniform core, the guided mode of the entire structure is characterised by a transverse resonance condition $f_{TR}(k_0, k_{y1}, k_{y2}, k_z, d) = 0$. Its explicit expression can be found in the literature [9, 12]. Briefly, it originates from the conservation of k_z at the two interfaces parallel to z and the continuity of the appropriate field components of evanescent modes in the semi-infinite homogeneous regions and propagating Bloch modes in the section of the 1D grating region. Considering frequency values around the first order stop-band, the grating allows at most two propagating Bloch modes (with transverse wave-vectors k_{y1} and k_{y2}). Proof of this can be found in Fig. 6 where a horizontal line (at constant k_0) would intercept the band-edge curves at most in two points.

Since the transverse resonance relation implicitly includes the dispersion relations of the modes existing in the three adjacent regions, the considerations on the properties of the Bloch modes of the 1D grating can be extended also to the Bloch modes of the 2D structure. Given the solution $(k_0, k_{y1}, k_{y2}, k_z, r)$ of $f_{TR} = 0$, the Bloch mode i obeys the Brewster condition if k_0 and k_{yi} are related by Eq. (2). If the Bragg condition $k_z = K/2$ is also satisfied, then $k_{y1} = k_{y2} = k_{yB}$ — and the stop-band closes at k_{0B}.

Figure 7 shows the dependence of the stop-band edges on the slab thickness d, calculated following the two wave approximation [9] on a structure having $\Lambda = 0.390$ μm, duty cycle 0.5, $n_1 = 1$, $n_2 = 2.97$, $n_u = n_l = 1$, At $d = d_B \approx 0.563$ μm the stop-band edge-curves cross each other. This point corresponds to $k_{0B} = 0.3191K$, consistently with Eq. (3). As for stacked 1D structures, the intensity maps ($|H_x|^2$) of the standing waves also undergo a $\Lambda/2$ shift across the closure point (insets of Fig. 7).

With the simple drawing of a symmetry plane below the bottom horizontal interface and at a distance $(w/2) - d$ from it, this type of structure can be transformed into the 2D top-view PhWBG geometry shown in Fig. 5(d) [6]. Note that in the figure the thicker line highlights the contour of the PhWBG geometry which, considering the refractive indices $n_1 = n_u$ and $n_2 = n_l$, becomes the same device as shown in the inset of Fig. 1. Also, note the consistency of the symbols in both Fig. 5 and Fig. 1.

The considerations made so far apply also to this case: we can find a stop-band closure at $k_0 = k_{0B}$ that is completely defined by the properties of the 1D grating. The relevant values of w and d, however, depend on the transverse resonance condition, therefore are found solving

#107611 - $15.00 USD Received 17 Feb 2009; revised 2 May 2009; accepted 4 May 2009; published 12 May 2009

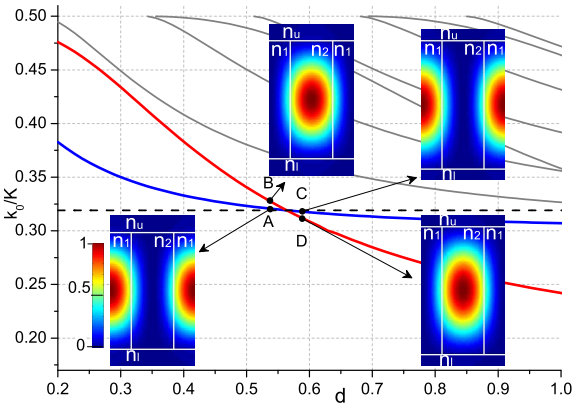

Fig. 7. Stop-band edges of various orders in dependence of the grating thickness d, calculated with a two-wave approximation of the dispersion relation. The insets show the intensity maps ($|H_x|^2$) for four points around the stop-band closing condition at $d_B \approx 0.563$ μm. Points A and B have $d = 0.538$ μm, whereas points C and D have $d = 0.59$ μm. The dashed horizontal line represents $k_{0B} = 0.3191K$ evaluated by Eq. (3).

the dispersion relation fully. We can also find inversion of the intensity configurations ($|H_x|^2$), as is shown by Fig. 8, where dispersion curves k_0 *vs.* k_z are shown that are calculated using an eigen-mode expansion technique [13], using the same geometry of the previous case, and setting $w = 500$ nm. The stop-band appears closed for $d = 184$ nm, at $k_0 = 0.288K$, which is $\approx 10\%$ off the theoretical value already mentioned $k_{0B} = 0.3191K$. This difference is due to the limited number of plane waves used in the calculation.

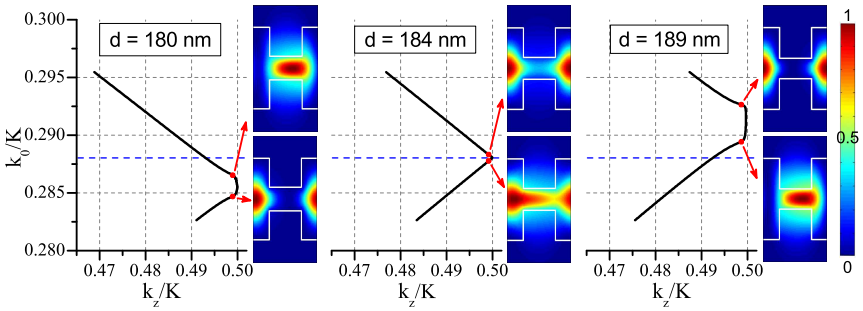

Fig. 8. Dispersion curves and intensity plots ($|H_x|^2$) at the stop-band edges for three values of recess depth d, around the configuration that results in the stop-band being closed ($d = 184$ nm) at $k_0 = 0.288K$. The intensity maps are calculated at $k_z = 0.4989K$.

Finally, a complete 3D PhWBG (Fig. 1) can be obtained when a transverse confinement condition along the x direction is added. Note that for the 3D case the definition of TE and TM polarizations changes so that TE (TM) has the E (H) component mainly along y rather than along x. Again the dispersion equation is found by posing the continuity of the appropriate field components at the interfaces. The important effect which occurs now is that pure TE and TM modes no longer exist, but they become hybrid, i.e. they have all six components not null, although they exhibit quasi-TE and quasi-TM characteristics.

The presence of field components belonging to both 2D polarizations within a single hybrid mode suggests that in the 3D case the stop-band closure effect may be affected. Since a com-

#107611 - $15.00 USD Received 17 Feb 2009; revised 2 May 2009; accepted 4 May 2009; published 12 May 2009

plete theoretical description appears not possible in the simple terms used so far, in the present analysis we note that the 3D FDTD and experimental results demonstrate evident stop-band shrinkage.

We can compare the results of the 3D FDTD simulations to those of the theoretical model. Considering the 1D grating relevant to the 3D structure made by alternating layers of air ($n_1 = 1$) and silicon ($n_2 = n_{Si} = 3.479$) with period $\Lambda = 390$ nm and duty cycle 0.5 (compare Fig. 5 and the considerations in the previous paragraph) — Eq. (3) can be used to evaluate the wavelength at which the stop-band should be closed — yielding $\lambda_B = 1411.7$ nm. This value is only $\approx 1\%$ off the simulation result ≈ 1420 nm reported in Fig. 4, thus confirming the validity of the theoretical model.

The last result left to be explained is the inversion of the slope of the loss curve around the stop-band closure geometry, observed in the 3D finite length grating (Fig. 3). Recalling the results of a previous publication [6], the power scattered by a PhWBG having photonic wire feeder waveguides is due only to the modal distribution mismatch at the interface between the two structures. When the Bloch mode of the PhWBG is mainly located in the wider part of the grating (the teeth) its shape is similar to that of the input/output photonic wire waveguides — and the interface mismatch (i.e. loss) is minimal. Conversely, when the Bloch mode is shifted so as to be located mainly in the narrower part of the grating, the losses are larger. Therefore, the inversion of the field patterns demonstrated as Brewster's condition is crossed causes the inversion of the slope of the loss curve.

This analysis also suggests that the band-gap closure does not arise in structures with circular holes. In that case, the curved surface of the hole should prevent the occurrence of the Brewster's condition for the whole mode.

All the considerations developed so far show rigorously the reasons for the band-gap closure and provide tools for the design of a structure exhibiting this effect. The useful feature of the proposed model consists in the possibility of determining the band closure condition simply by studying a 1D stack structure without the need to solve the complicated 3D dispersion equation. However, if the actual geometry is sought, the full dispersion relation has to be considered. It is anyway worthwhile to note that this effect is quite general and can be observed in other types of structure, which will be shown in the next section, where a simple transmission line model will be used to replicate the effects discussed so far.

4. Band-gap closure and transmission lines

In this section we shall highlight the essential features of the band-gap closure phenomenon by showing how to include it in the design of a structure. To do this, we move to the context of transmission lines because it represents a simple and general model for a guided-wave system. The large applicability of the transmission line model to many types of wave-guiding structures suggests also that the phenomenon may be designed in other technologies.

The phenomenon of stop-band closure has been understood as the result of the simultaneous satisfaction of two independent conditions: a local one i.e. the absence of reflections at each discontinuity, and a global one, i.e. the Bragg condition, that is the synchronism between the mode and a periodic structure.

The first step of the design is the identification of a finite length structure, the reflectivity of which can become null at a wavelength λ_0. Figure 9 shows three possible implementations of such a structure. Figure 9(a) shows a cascade of transmission line sections having characteristic impedance Z_0 and Z_1, separated by matching sections having characteristic impedance $Z_m = \sqrt{Z_1 Z_2}$ and length l. The total length of the structure is Λ. When the wavelength becomes such that $l = \lambda_0/4$, all sections are matched to one another. In Fig. 9(b) the structure is implemented as a section of transmission line having characteristic impedance Z_0 and length Λ. The line is

#107611 - $15.00 USD Received 17 Feb 2009; revised 2 May 2009; accepted 4 May 2009; published 12 May 2009

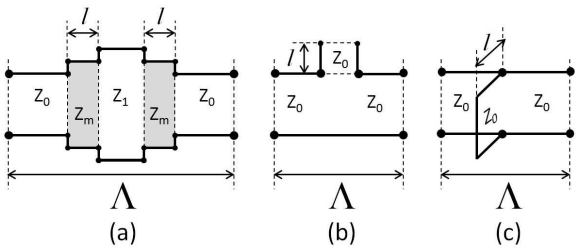

Fig. 9. Three transmission line configurations that can result in stop-band closure.

loaded by an open-circuit stub in series having length l and characteristic impedance Z_0. Its input impedance becomes null at $l = \lambda_0/4$, making its reflectivity also null. In Fig. 9(c) the implementation consists of a section of transmission line having characteristic impedance Z_0 and length Λ. The line is loaded by a short-circuit stub in parallel made by a line having length l and characteristic impedance Z_0. Its input impedance becomes infinite at $l = \lambda_0/4$, making its reflectivity null.

In the following we concentrate on the structure of Fig. 9(c) simply because it is frequently used in practice. However, any of these implementations could be employed, leading to similar results. Considering the closed-circuit parallel stub, we note that when $0 < l < \lambda_0/4$ the stub acts like a lumped inductor, its impedance being positive. When $\lambda_0/4 < l < \lambda_0/2$ the stub acts like a lumped capacitor, its impedance being negative. The change of sign of the impedance causes a shift of π in the reflected wave.

The second condition for obtaining band-gap closure is to set the Bragg condition at the design wavelength λ_0, through $\Lambda = \lambda_0/2$. In the structure obtained by repetition of the period unit, when the stub length is such that at λ_0 it acts as an open circuit ($l = \lambda_0/4$), the stop-band cannot form because of the absence of reflections.

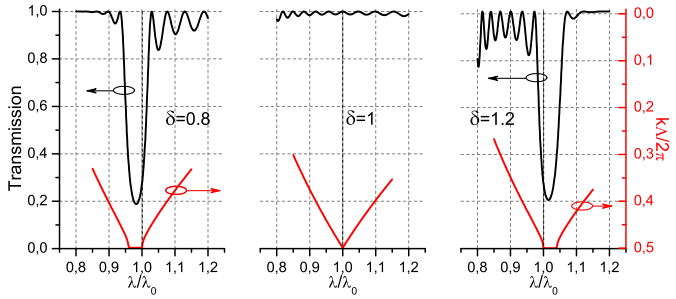

Fig. 10. Calculated transmittance (black) and dispersion curves (red) of the transmission line loaded by 10 short-circuit stubs as a function of the normalised stub length $\delta = l/(\lambda_0/4)$.

This result is shown in Fig. 10 which reports calculations of the spectral characteristics of the transmittance (black) and of the dispersion curves (red) of the transmission line loaded by 10 stubs, as a function of the normalised stub length $\delta = l/(\lambda_0/4)$. Note that the wavelength axes are also normalised with respect to λ_0.

The behaviour of this structure is similar to that described for the dielectric gratings: when δ approaches 1, the dispersion curves define a gap with decreasing width. The transmittance of a finite length device shows reducing minimum transmittance up to the point of complete

#107611 - $15.00 USD Received 17 Feb 2009; revised 2 May 2009; accepted 4 May 2009; published 12 May 2009

gap closure, at $\delta = 1$. This structure also shows an inversion of its behaviour that is visible through the swapping of the Bragg oscillations symmetrically, with $\delta = 1$. These oscillations are a Fabry-Perot like effect at the ends of the periodic structure. Their visibility increases when its 'effective impedance' is farther from the impedance of the line. This swap in the effective impedance is analogous to the swap in the field shape (and therefore in the effective index) at the stop-band edges of the dielectric gratings.

5. Conclusions

We have demonstrated experimentally and computationally that photonic wire Bragg gratings retain a larger degree of complexity than gratings made with small corrugation. By increasing the index modulation it is possible to cancel their reflectivity and swap the field configurations at the stop-band edges. We have related this phenomenon to the incidence of the field at planar discontinuities at the Brewster angle. The theoretical model that we have developed makes it possible to determine the analytical expression for the wavelength at which this phenomenon is observed, simply by referring to a 1D stacked grating. Making use of the reduction and change of sign of the reflection coefficient in each cell of a periodic transmission line structure, we have reproduced the same phenomenon within a transmission line model. This effect, which has not been reported for hole-based photonic wire gratings, could be used to make sensing or nonlinear devices or wire-grating taper sections that can provide gradual mode shape tapering without coupling power to back-propagating modes.

A. Single interface at Brewster's incidence

Considering the interface between the two homogeneous media depicted in Fig. 5(a), a TM polarised plane wave impinges at Brewster's angle when its incidence angle α_1 and transmission angle α_2 satisfy the relation $\alpha_1 + \alpha_2 = \pi/2$. For this condition, the reflection coefficient is zero. Equation (1) can therefore be cast as:

$$\tan(\alpha_1) = n_2/n_1 \tag{4}$$

where n_1 and n_2 are the refractive indices of the materials. The incidence angle α_1 can also be related to the propagation constants by

$$\tan(\alpha_1) = \frac{k_y}{k_{z1}} = \frac{k_y}{\sqrt{k_0^2 n_1^2 - k_y^2}} \tag{5}$$

where the last equality holds because medium one is homogeneous. By equating relations (4) and (5), the propagation constant parallel to the material interface, k_y, can be written as being proportional to the vacuum propagation constant k_0 according to Eq. (2).

B. One-dimensional grating at Brewster's incidence

Considering the 1D grating depicted in Fig. 5(b), the dispersion relation, found with a transfer matrix approach can be written as:

$$f_{1D}(k_0, k_y, k_z) \equiv \cos(\Lambda k_z) - (A+D)/2 = 0\,, \tag{6}$$

#107611 - $15.00 USD Received 17 Feb 2009; revised 2 May 2009; accepted 4 May 2009; published 12 May 2009

where A and D are the diagonal elements of the relevant 2x2 translation matrix [8], which, for TM polarization, can be written as:

$$A_{TM} = e^{jk_{z1}a}\left[\cos(k_{z2}b) + j\frac{1}{2}\sin(k_{z2}b)\left(\frac{n_2^2}{n_1^2}\frac{k_{z1}}{k_{z2}} + \frac{n_1^2}{n_2^2}\frac{k_{z2}}{k_{z1}}\right)\right] \tag{7a}$$

$$D_{TM} = e^{-jk_{z1}a}\left[\cos(k_{z2}b) - j\frac{1}{2}\sin(k_{z2}b)\left(\frac{n_2^2}{n_1^2}\frac{k_{z1}}{k_{z2}} + \frac{n_1^2}{n_2^2}\frac{k_{z2}}{k_{z1}}\right)\right] , \tag{7b}$$

where a and b are the thicknesses of the layers of the 1D grating having refractive index n_1 and n_2, respectively — and k_{z1} and k_{z2} depend directly on k_y and k_0.

For any given pair (k_y,k_z) [or (k_0,k_z)], the k_0 (or k_y) values that solve the dispersion relation (6) belong to a discrete set. An example of this at the Bragg condition ($k_z = K/2$), for the lowest order mode, can be found in Fig. 6, where a vertical line (at constant k_y) intercepts the TM (or TE) curves in two points having distinct k_0 values. When Brewster's condition is approached, the two curves cross and the dispersion relation has only one solution, k_{0B}.

In Fig. 6, the dispersion relation was firstly solved numerically by posing the Bragg condition and then analyzed for the stop-band edge behaviour at Brewster's condition. However, in order to find the analytical expression of the stop-band closure point it is convenient to firstly impose the Brewster's condition and then the Bragg condition, because it simplifies expression (6) greatly.

Therefore, inserting Eqs.(2) and (5) into Eqs. (7), the dispersion relation (6) becomes:

$$\Lambda k_{zB} = \eta k_{yB} + 2m\pi , \tag{8}$$

where $\eta = \frac{n_2}{n_1}a + \frac{n_1}{n_2}b$ and m is an integer number. In order to find the wave-numbers corresponding to the stop-band edges k_{0B}, we consider the Bragg condition by imposing $k_z = K/2$, thus obtaining:

$$k_{0B} = \frac{\pi + 2m\pi}{\eta\, n_B} . \tag{9}$$

This relation shows that for any given stop-band order m, the stop-band edges at the Brewster's condition have degenerated into a single value k_{0B}, from which the frequency values ω of the stop-band disappearance can be calculated.

Acknowledgments

The authors acknowledge Ronald Dekker for invaluable help. Partial funding for this work is acknowledged — from the UPC and ePIXnet projects, the ProMiNER Project for Micro and Nano Technologies in Emilia-Romagna, and NanoNed, a national nanotechnology program coordinated by the Dutch ministry of Economic Affairs.